J Infrared Milli Terahz Waves (2010) 31:1171–1181
DOI 10.1007/s10762-010-9693-1

RDX Detection with THz Spectroscopy

Zoi-Heleni Michalopoulou · Suman Mukherjee · Yew Li Hor · Ke Su · Zhiwei Liu · Robert B. Barat · Dale E. Gary · John F. Federici

Received: 19 February 2010 / Accepted: 27 July 2010 /
Published online: 6 August 2010

Abstract Spectroscopic analysis in the Terahertz frequency range, providing characteristic "signatures" for explosive and non-explosive materials, is proposed as an efficient and powerful tool for explosive identification. It is demonstrated that spectral responses of materials can be used as fingerprints that distinguish cyclotrimethylenetrinitramine (RDX) from other materials even with simple detectors and a limited number of available frequencies. Detection is performed using a modified least squares approach and multilayer perceptrons that operate on smoothed reflectance spectra. The performance of the detectors is evaluated through application to spectra of RDX and several common materials. A Receiver Operating Characteristic curve analysis demonstrates that our detectors exhibit the desirable properties of high probability of detection and low probability of false alarm.

Keywords THz spectroscopy · Explosive detection · Neural networks · ROC curves

1 Introduction

The urgent need for extensive, reliable, and fast screening for the identification of explosives stemming from public safety and homeland security concerns has stimulated the search for efficient, quantitative, and reliable detectors and classifiers. Terahertz (THz) spectroscopy has been proposed as a valuable tool to this end [1–10]. It is a particularly useful approach because lethal agents have distinct spectral signatures in the THz frequency

Z.-H. Michalopoulou (✉)
Department of Mathematical Sciences, New Jersey Institute of Technology, Newark, NJ 07102, USA
e-mail: michalop@njit.edu

S. Mukherjee · Y. L. Hor · K. Su · Z. Liu · D. E. Gary · J. F. Federici
Department of Physics, New Jersey Institute of Technology, Newark, NJ 07102, USA

R. B. Barat
Otto York Department of Chemical Engineering, New Jersey Institute of Technology, Newark, NJ 07102, USA

range that can serve as "fingerprints" for their identification, while most common dielectric barriers are largely transparent to THz radiation.

In [2], we applied multilayer perceptrons and Kohonen Self Organizing Maps to simulated images of RDX (cyclotrimethylenetrinitramine) and metal, synthesized with THz synthetic aperture / interferometric imaging. The networks successfully separated the two categories of materials in distinct classes. In [6], the presence or absence of agents such as RDX was detected by a least-squares difference calculation between measured and reference reflectance spectra in the THz range. The approach was supported by analysis of RDX spectra measured in the lab, clearly indicating a common spectroscopic behavior across several different scans of RDX. Classification of materials and identification of RDX was straightforward when reflectance level was taken into account.

True reflectance level, however, being susceptible to attenuating barriers and calibration factors, cannot be accurately linked to a specific material and cannot solely form an identifying feature. Removing the true reflectance level results in identification based only on shape of spectroscopic curves across frequency. Preliminary work in [6] demonstrated that relative levels can indeed be employed for RDX identification, with an increase in probability of false alarm being the penalty of identification based only on shape.

Explosive identification was pursued in [8, 9], employing reflectances in the THz range as well. Transforming reflectance to absorption, classification was possible by matching absorption peaks to known material characteristics.

In this paper, we extend our work [2, 6] and explore how a priori information on shapes of spectral signatures of materials in the THz range can be utilized for the implementation of a robust explosive detector-classifier when measurements at a few frequencies (13 and 7) are available. We use a modified least-squares detector and multilayer perceptrons [11] and demonstrate that preprocessing the spectra by approximating them with splines [12] improves detection performance.

The paper is organized as follows. Section 2 briefly describes the data acquisition process and our measurements. Section 3 presents a preprocessing smoothing step implemented before detection. In Section 4, multilayer perceptrons are employed in RDX detection. Section 5 shows least-squares detection results and presents a constrained least-squares processor that emphasizes spectral shape as a feature. Conclusions are presented in Section 6. Analysis was performed with MATLAB® and the spline routines developed in [15].

2 Data acquisition

THz transmission and reflection spectra are measured using a Picometrix T-Ray 2,000 THz time-domain spectrometer (THz-TDS). With the THz-TDS, the time-domain THz pulse is measured. The roughly 80 ps waveform is converted to the frequency domain via a Fourier transform. The usable frequency band is typically 0.1–2 THz. Details of the THz-TDS method can be found in [4, 13].

The probing THz radiation is focused using silicon lenses to roughly a 3 mm spot size on the sample. Reflection measurements from C4 explosives (a pliable matrix consisting of 91% RDX by weight, with a balance of spectrally inert plasticizer, binder, and lubricant) are performed on optically thick samples ensuring that the reflected THz waveform is due only to specular reflection from the front surface of the sample. Transmission measurements on thin samples reveal a pronounced absorption peak near 0.8 THz [4]. In reflection, the

presence of the absorption peak appears as a change of reflectance near 0.8. Specifically, the reflection of electromagnetic radiation from the surface of a material can be characterized by the Fresnel equations. For simplicity, consider the reflection coefficient at normal incidence:

$$R = \left(\frac{1-\widetilde{n}}{1+\widetilde{n}}\right)^2 \tag{1}$$

where $\widetilde{n}(\omega) = n_r(\omega) + i\, n_i(\omega)$ is the frequency-dependent complex refractive index of the material. Spectral regions in which there is a large peak in the absorbance produce a strong frequency dependence in the imaginary index of refraction. Since changes in the imaginary refraction index are manifested in the reflectivity according to Eq. (1), there will be a corresponding change in reflection with frequency spectral regions of strong absorption peaks. Thus, the absorption peak of RDX at around 0.8 THz will appear as a "drop" in reflectance at that frequency.

The reflectance is measured at multiple locations in order to sample the variation in measurements due to material inhomogeneity and changes in surface topology. A gold mirror is used as reference.

It was of particular interest to study the performance of the proposed classifier-detector as a function of the number of frequencies at which reflectance measurements are available. Our data consist of reflectance measurements between 0.6 and 0.9 THz at thirteen and seven frequencies; RDX detection is performed for both and the goal is to study the limitations imposed by the number of frequencies. The thirteen frequencies are 0.600, 0.625, 0.650, 0.675, 0.700, 0.725, 0.750, 0.775, 0.800, 0.825, 0.850, 0.875, and 0.900 THz; 0.600, 0.650, 0.700, 0.750, 0.800, 0.850, and 0.900 THz are the seven frequencies. The study of RDX detection as a function of the number of frequencies is motivated by our plan to develop a fast interferometric CW imaging system in the THz range [14], which is practical to implement at a limited number of frequencies.

In order to remove calibration effects and retain only shape information, all spectra were normalized to unit-norm vectors before being used for training and testing of detection approaches.

3 Spline smoothing of reflectance spectra

As noted in [15], data preprocessing is a powerful tool for improving the performance of a learning algorithm. To facilitate the explosive detection procedure, we follow the approach proposed by Zorych *et al.* [12] and preprocess data by extracting smooth shape information from the measured reflectance spectra in the THz frequency range.

For each material of interest, reflectance measurements are made in a specified frequency range; data consist of pairs $\{(\omega_k, s_k)\}$, k=1, 2, ..., K, where ω_k is a frequency and s_k is a measurement of reflectance at that frequency. The pair can be represented as:

$$s_k = f(\omega_k) + \varepsilon_k, E(\varepsilon_k) = 0, \tag{2}$$

where ε_k is a random error and $E(\varepsilon_k)$ is its expectation; experimentation has shown that a zero-mean Gaussian model for ε_k is a reasonable assumption. The goal here is to estimate function f from data pairs $\{(\omega_k, s_k)\}$, k=1, 2, ..., K, in a way that facilitates the extraction of shape information from the THz spectrum.

A spline $f(\omega)$ may be expressed as follows:

$$f(\omega) \approx \sum_{j=1}^{M} \beta_j \varphi_j(\omega), \tag{3}$$

where $\{\varphi_j\}$, $j=1, 2, ..., M$, form a set of basis functions, and β_j, $j=1, 2, ..., M$, are coefficients that combine the basis functions to build f. In this paper, we use splines of degree 2: 1, ω, ω^2. Second-degree splines enable us to fit a model using only a limited number of THz frequencies at which measurements are available. Higher degree splines may lead to overfitting.

Figure 1 illustrates two RDX reflectance spectra sampled at thirteen equally spaced frequencies between 0.6 and 0.9 THz and their spline approximations; the spectra are measured in the lab with the T-Ray system. As previously discussed and also demonstrated by the figure, the spline representation has a smoothing effect on the measured spectra, which is helpful for successful classification [12]; spline representations closely follow the shape of the mean RDX spectrum. In a similar fashion to Fig. 1, Fig. 2 depicts THz spectra of bubble wrap and cardboard and corresponding approximations with splines. We see that the smoothed RDX spectra of Fig. 1 are very similar, having the characteristic "drop" in reflectance level at around 0.8 THz, also seen in [6, 8], because of the RDX absorption peak at 0.82 THz. The spectra of Fig. 2, corresponding to non-RDX materials, do not have the characteristic shape seen in Fig. 1. This shape "signature" of RDX reflectance is the feature that we explore in this work.

Spectra of both Figs. 1 and 2 exhibit a peak near 0.77 THz, which is the result of residual water vapor absorption because of water presence in the air. Although a dip would be intuitively expected in reflectance measurements at 0.775 THz because of water

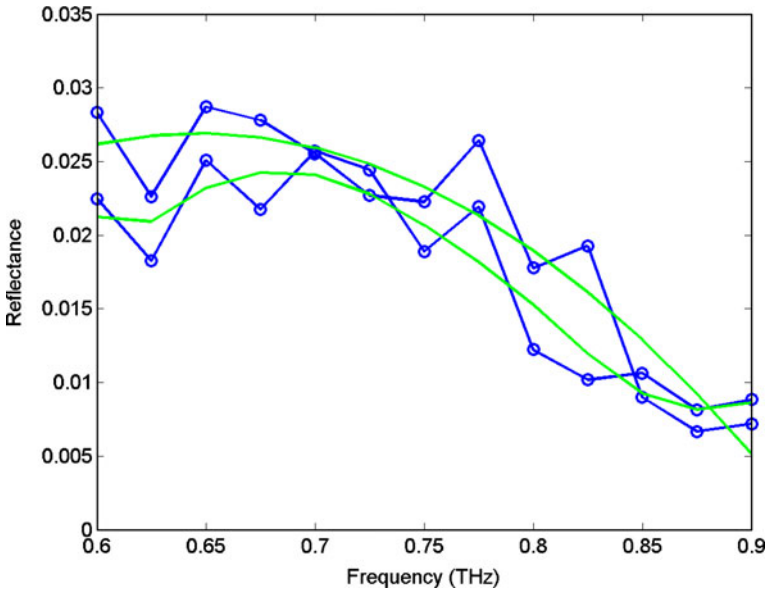

Fig. 1 (color online) RDX spectra from two scans at thirteen frequencies between 0.6 and 0.9 THz (*circles*) and corresponding approximations with splines (*solid lines*). The consistent peak near 0.77 THz is from residual water vapor absorption because of water presence in the air.

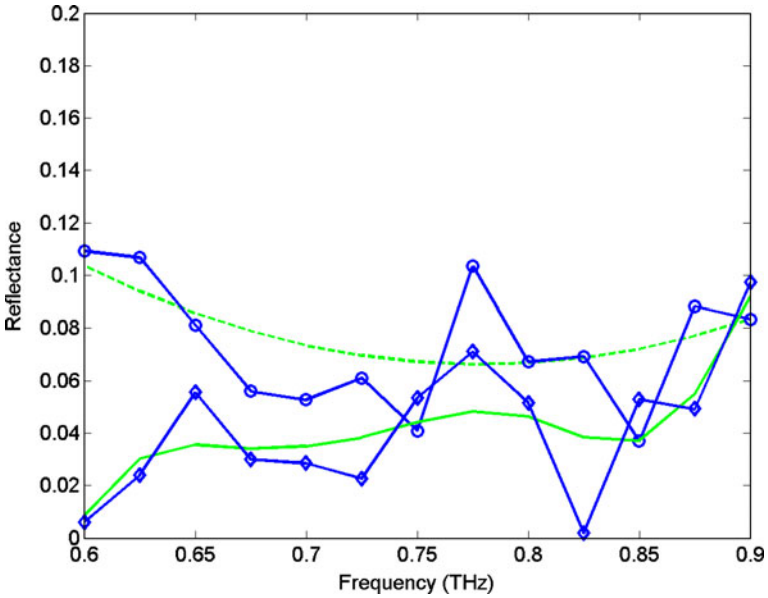

Fig. 2 (color online) Spectrum of bubble-wrap plastic at thirteen frequencies between 0.6 and 0.9 THz (*circles*) and corresponding approximation with splines (*dashed line*); spectrum of cardboard (*diamonds*) at thirteen frequencies between 0.6 and 0.9 THz and corresponding approximation with splines (*solid line*). Similarly to Fig. 1, the peak near 0.77 THz is from residual water vapor absorption.

absorption at that frequency, a peak is often observed instead. The presence of the peak is the result of reflectance calculation as the ratio of the reflected field from the material of interest over the reflected field from a reference (gold mirror in our case). The division can lead to a large number generating a peak, when the denominator has a small value because of water vapor absorption.

4 RDX detection with multilayer perceptrons

To identify RDX from other materials, a detection scheme is required. We implement here a multilayer perceptron with reflectance spectra being the input patterns. The network has one hidden layer. The output layer consists of a single node which is trained to obtain values of 1 or −1 when it is presented in the training stage with RDX or non-RDX vectors respectively. The network was trained with a gradient descent algorithm.

A total of 2115 reflectance spectra are available; out of those, 284 are reflectance spectra from RDX. The RDX set of data patterns consists of 56 spectra from a thin sample, 28 patterns from the same sample placed behind four barriers (plastic ruler, duct tape, cardboard, cloth), 100 samples from a second thicker sample, and 100 samples from the latter sample placed behind a leather barrier. The non-RDX set consists of spectra from plastic, cardboard, cloth, flour, and sugar. The complete data set is divided in two groups: training and testing; 1017 patters are used for training and 1098 patterns are employed in testing the detector. To evaluate the ability of the detector to generalize in identifying correctly RDX under a variety of circumstances, the training set does not contain any spectra from RDX behind a barrier; instead it contains 50 patterns from each RDX sample;

the network is then presented with spectra of RDX behind barriers during the testing stage. With this constraint in place, the division into the two groups—training and testing—is performed randomly. The process of separating the patterns is carried out five times for five-fold cross-validation; that is, the set of available spectra is divided randomly five different times into training and testing subsets to ensure generalization of the process.

Receiver Operating Characteristic (ROC) curves were constructed by selecting different threshold values for the processor output and computing for each value the probability of correct RDX identification (probability of detection) and probability of incorrectly identifying benign materials as RDX (probability of false alarm). For low thresholds both probabilities are expected to be high (reaching the top right corner of the figure); for large threshold values, these probabilities are very small (close to the bottom left corner). It is of particular interest to observe the probability behavior for intermediate threshold values. The ideal situation is to have, for certain thresholds, a high probability of detection coupled with a low probability of false alarm (with the ROC curve approaching the top left corner of the plot).

Figure 3(a) demonstrates ROC curves for the results of the multilayer perceptron with raw 13- frequency spectra and with spectra smoothed with splines, as described in Section 3; results for seven frequencies are presented in Fig. 3(b). Fig. 3(a) shows that the perceptron results are very good with smoothed, 13-frequency spectra, with probability of detection at a level of 92% for a 10% probability of false alarm. Raw data results are different; the ROC curve in that case shows inferior detection.

Performance deteriorates with seven available frequencies for each spectrum, with probability of detection at a level of 85% for a 10% probability of detection.. The classification with raw data is inferior with a probability of detection of 76% at the same false alarm level. Comparing the raw data ROCs in Fig. 3(a) and (b), it can be seen that the classifier performs worse in the 13 frequency case than in the seven frequency case when raw spectra are employed. This observation is counterintuitive; we expected that data at 13 measurements would provide better detection results than those with spectra at 7 measurements. The results can be explained by the fact that the thirteen frequencies include 0.775 THz, which is very close to a water absorption line. Around such frequencies, artifacts may be observed in reflectance spectra, which can be manifested as peaks such as the ones seen in Figs. 1 and 2 as also previously discussed. When splines are used, the peaks due to the water lines are smoothed away and do not present a problem, improving

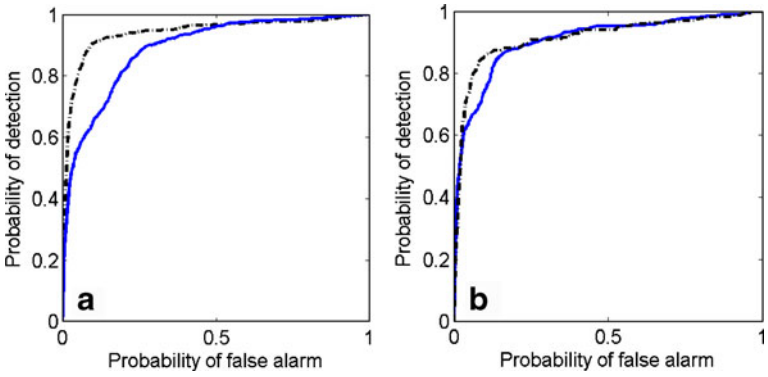

Fig. 3 (color online) ROC curves for testing the multilayer perceptron on smoothed data (*dot-dashed lines*) and raw data (*solid lines*) for (**a**) 13 and (**b**) 7 frequencies.

the performance as demonstrated by the ROC curve (dot-dashed line) of Fig. 3(a). It should be noted here that for both the 13 and seven-frequency unprocessed data cases, some of the neural network validation runs produced good results. However, performance of different runs was variable; there were instances where the networks could not converge during learning. Detection that incorporated the preprocessing stage produced more robust results that were only negligibly varying between cross-validation runs.

It can be observed from Fig. 1 that splines remove only water peak effects without affecting the general RDX spectral characteristics. This is because the RDX reflectance peak around 0.8 THz is a feature extended over a number of frequencies that is well approximated functionally using splines. On the other hand, artifacts such as the sharp peaks near 0.775 THz cannot be represented well by a smooth spline expression with suitable knots, presenting oddities that the splines do not follow.

5 RDX detection with least squares

A least squares processor was also designed for RDX detection. The processor calculated the squared differences (errors) between testing patterns and reference patterns for RDX and other available materials. Reference patterns were mean spectral signatures extracted from the training data sets (the data were divided in training and testing subsets exactly as in Section 4). The minimum difference between each test pattern and all non-RDX (nRDX) references was subtracted from the difference between the pattern and RDX reference. Specifically, for every pattern $f(\omega)$, differences d_{RDX} and d_{nRDX} are calculated as:

$$d_{RDX} = \sum_{j=1}^{N} \left(f\left(\omega_j\right) - ref_{RDX}\left(\omega_j\right) \right)^2 \tag{4}$$

$$d_{nRDX} = \min\left(\sum_{j=1}^{N} \left(f\left(\omega_j\right) - ref_{nRDX_1}\left(\omega_j\right) \right)^2, \sum_{j=1}^{N} \left(f\left(\omega_j\right) - ref_{nRDX_2}\left(\omega_j\right) \right)^2, \ldots, \sum_{j=1}^{N} \left(f\left(\omega_j\right) - ref_{nRDX_K}\left(\omega_j\right) \right)^2 \right) \tag{5}$$

where ref_{RDX} is the reference pattern for RDX and ref_{nRDXi}, $i= 1,...,K,$ are reference patterns for K non-RDX materials. Difference d is computed as

$$d = d_{RDX} - d_{nRDX}. \tag{6}$$

Decisions are made based on the value of d, the detection statistic in our case; the smaller its value, the more likely it becomes for the pattern to belong into the RDX class.

Figure 4 (a) presents the ROC curve obtained for 13-frequency unprocessed spectra for the least squares detector (red dotted curve) and the corresponding results after processing with splines (green dashed curve); the curves are superimposed on the perceptron results for comparison (black dot-dashed curve). The performance of the detector after the spline preprocessing step is satisfactory in that large probability of detection is obtained for small probabilities of false alarm but is inferior to that of the multilayer perceptron.

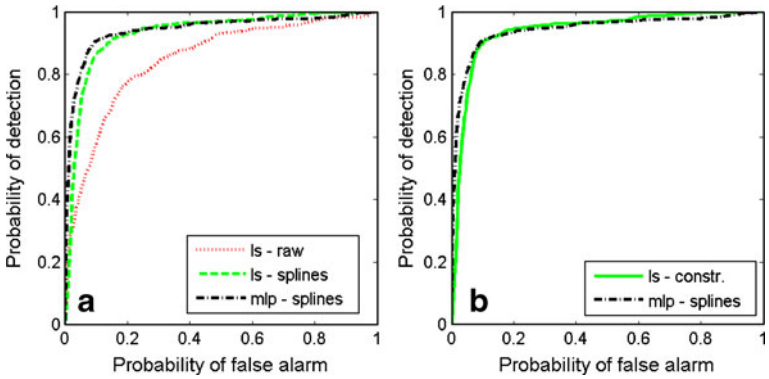

Fig. 4 (color online) (**a**) ROC curves for the least squares detector applied to 13-frequency raw data (*red dotted curve*) and to smoothed data (*green dashed curve*), superimposed on the ROC curve for the neural network applied to smoothed data (*black dot-dashed curve*); (**b**) ROC curves for the least-squares processor with constraints (*green solid curve*) and the multilayer perceptron (*black dot-dashed curve*).

Least-squares is a powerful and simple detection/estimation tool. Relying on a simple distance measure between measured and reference spectra, it does not take into consideration the shape of the pattern in question. To remedy that, we propose a modified least squares processor that incorporates shape information; this approach is similar to the multiple expert method of [16]. Our detection statistic d takes the form:

$$d = d_{RDX} - d_{nRDX} + l_1 \text{constraint}, \tag{7}$$

where l_1 is a positive regularization coefficient. We see in Fig. 1 that smoothed RDX spectra have steeper changes in the 0.7–0.9 THz interval rather than in the 0.6–0.7 THz range. The constraint in our case is, thus, that the slope of the spectrum is large in the 0.6–0.7 THz range and, more specifically, larger than in the 0.7–0.9 THz range, a feature unlikely to appear in RDX data; comparisons are made in terms of absolute values. If this is true for a pattern under investigation, statistic d will obtain larger values that it normally would without the constraint in place, "pushing" the decision towards non-RDX. Coefficient l_1 is determined during the training process, by searching for the value of l_1 that provides the highest probability of detection for a chosen probability of false alarm. If, during training, the optimal value of l_1 is estimated to be zero, it means that the constraint does not provide any additional information to the detector. Values other than zero indicate that the selected constraint reflects true data characteristics. In our implementation, this was found to be the case. ROC curves for the 13-frequency smoothed data as calculated by the new least squares detector are shown in Fig. 4(b) (green solid line), demonstrating that the least squares performance has significantly increased with the shape feature taken into account in the detection process. Perceptron and modified least squares provide almost identical ROC curves especially at the level of 10% for false alarm.

Figure 5 shows estimated probability distributions of detection statistic d under the RDX and non-RDX hypotheses as calculated by (a) the least squares application to raw data and (b) the constrained least squares applied to smoothed data. The more separated these distributions are, the easier the detection task becomes, with data clearly mapped to RDX or non-RDX classes. We see that, in Fig. 5(b), there is a better separation between the two distributions than in Fig. 5(a), which leads to increased probability of detection and reduced probability of false alarm; that is, when the shape constraint is imposed and the data have been smoothed, RDX detection is more successful. This is because of the smoothing and

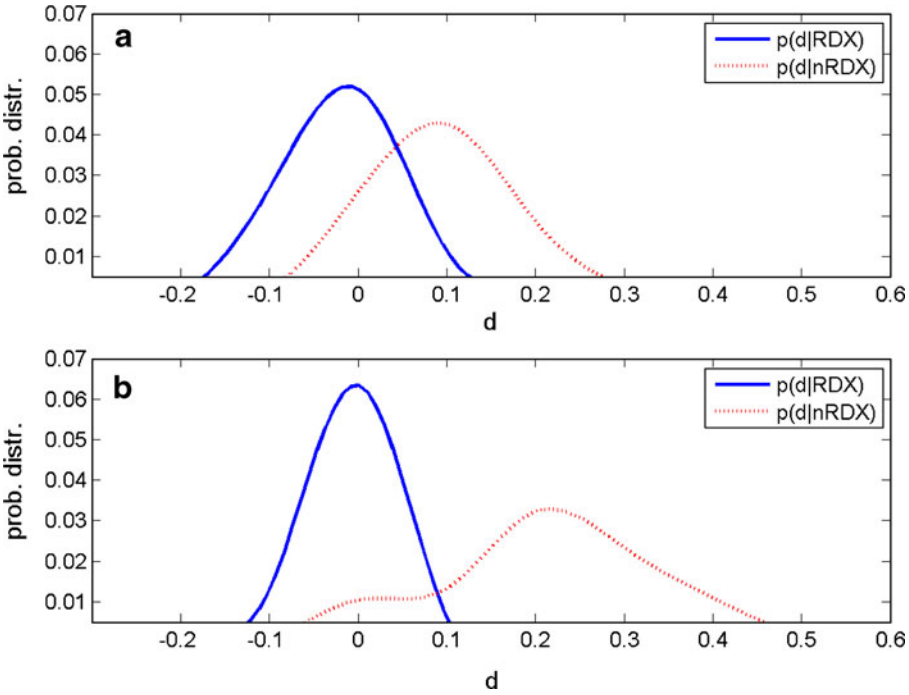

Fig. 5 (color online) (**a**) Probability distributions *p(d|RDX)* and *p(d|nRDX)* as calculated by the least squares processor applied to raw data for the thirteen-frequency case; (**b**) probability distributions *p(d|RDX)* and *p(d|nRDX)* as calculated by the least squares processor with constraints applied to smooth data for the thirteen-frequency case.

also because the constraint has "pushed" the distribution of d under the non-RDX hypothesis away from the distribution of d under the RDX hypothesis.

The seven-frequency results for the least squares processor with constraints are also interesting. Figure 6 demonstrates ROC curves for the proposed detector and the multilayer perceptron. The least-squares processor achieves a probability of detection of 90% at a false alarm level of 10%; for the same probability of false alarm, the neural network only reaches 85% correct detection. This is a marked improvement introduced via the constraints. There is a trade-off, however, because the probability of detection deteriorates for a probability of false alarm below 5%. Although the latter is an important factor to consider in detection, the potential of simple detectors with incorporated shape information is made evident.

6 Conclusions

Two detection methods are tested in processing reflectance measurements from materials in the THz frequency range for explosive agent detection. Our techniques are applied to measured reflectance data from various common materials including RDX, after first providing a functional approximation to each spectrum. This preprocessing step, based on the application of splines, produces a smooth representation of a typically noisy set of measurements. The smooth spectra representations are presented to a three layer perceptron and a least-squares detector for training and testing.

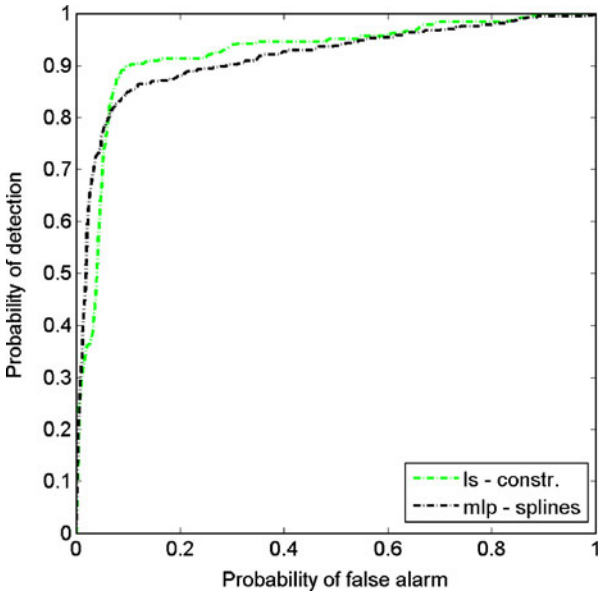

Fig. 6 (color online) ROC curves for the least-squares processor with constraints (*green solid curve*) and the multilayer perceptron (*black dot-dashed curve*) for the seven frequency case.

The multilayer perceptron is trained to assign data vectors to an "RDX" or "non-RDX" class. Conducting testing experiments on real data collected in our lab, our work confirms previous findings that spectroscopic information in the THz range is a powerful feature for material identification and quantifies the results with an ROC analysis. The classifier is characterized by the desirable properties of high probability of correct RDX detection and low probability of false alarm.

A least-squares detector is also tested. Although simple in its implementation, the least squares detector performs very well, especially when constraints representing RDX-specific shape information are incorporated in the decision function.

This work demonstrates the utility of at least two powerful tools in explosive detection in the THz range even when measurements at only seven frequencies are available; the success of the methods appears dependent on preprocessing the data to exploit structural information about spectral shape. This result is significant, making such approaches practical for real-time explosive detection, especially when they are combined with fast imaging. The improvement achieved by the feature information constraint in the least-squares approach is a promising result, showing that we can further improve detection, when we learn and incorporate specific shape features in our techniques.

The smoothing-preprocessing step employed in this work is found to play an important role in successful detection especially in the 13-frequency case; in that case, when raw spectra are employed, data at frequencies close to water vapor absorption lines can impact negatively detection results. There are indications that representing reflectance spectra with splines removes complications of water absorption.

The classification methods employed here, whether using raw or preprocessed data, try to identify a drop in the reflectance near 0.8 THz. One weakness of the approaches is that there is a possibility that other materials may exhibit a similar reflectivity spectrum to RDX near 0.8 THz; this may be more pronounced when measurements at a few frequencies are

used. However, these materials would have to exhibit not only a reflectivity drop at the correct THz frequency, but also one of an appropriate magnitude. For example, if a rough metallic surface exhibited a change in reflectance near 0.8 THz, the magnitude of reflection from the metal would be much larger than what one would expect from RDX, and could be classified as a non-RDX material based on that parameter as discussed in Ref.[6]. Materials could also be more accurately discriminated by including other spectral ranges for which strong absorbance peaks are manifested in RDX. However, there is an advantage to using a small spectral range: examining a small range increases the spectral scanning rate of the THz hardware.

Acknowledgment The authors gratefully acknowledge the funding support by Rajen Patel and the U.S. Army - Picatinny Arsenal EWMTD through grants DAAE3003D1015-22 and DAAE3003D1015-33.

References

1. Choi, M.K., A. D. Bettermann, D. W. van der Wiede, *Potential for detection of explosive and biological hazards with electronic terahertz systems.* Phil. Trans. R. Soc. Lond. A, 2004. **362**: p. 337–349.
2. Bandyopadhyay, A., A. Sengupta, R.B. Barat, D.E. Gary, Z.-H. Michalopoulou, and J.F. Federici, *Artificial neural network analysis in interferometric Terahertz imaging for detection of lethal agents.* International Journal of Infrared and Millimeter Waves, 2006. **27**(8): p. 1145–1158.
3. Federici, J.F., B. Schulkin, F. Huang, D. Gary, R. Barat, F. Oliveira, D. Zimdars, *THz imaging and sensing for security applications—Explosives, Weapons, and Drugs.* Semicond. Sci. Technol., 2005. **20**: p. S266–S280
4. Huang, F., B. Schulkin, H. Altan, J. Federici, D. Gary, R. Barat, D. Zimdars, M. Chen, D. Tanner, *Terahertz Study of 1,3,5-Trinitro-s-triazine (RDX) by Time Domain Spectroscopy and FTIR.* Appl. Phys. Lett., 2004. **85**: p. 5535–5537
5. Federici, J.F., D. Gary, R. Barat, Z.-H. Michalopoulou, *Detection of Explosives by Terahertz Imaging*, in *-Terrorism Detection Techniques of Explosives*, J. Yinon, Editor. 2007, Elsevier.
6. Zorych, I., A. Sinyukov, Z.-H. Michalopoulou, R. Barat, D. Gary, J. F. Federici. *Explosive identification with Terahertz spectroscopy: a model based approach*. in *SAFE 2007*. 2007. Washington, D.C.
7. Kemp, M.C., P. F. Taday, B. E. Cole, J. A. Cluff, A. J. Fitzgerald, W. R. Tribe, *Security applications of Terahertz technology*, in *Terahertz for Military and Security Applications*, D.L.W. R. J. Hwu, Editor. 2003, SPIE. p. 44–52.
8. Liu, H.-B., Y. Chen , G.J. Bastiaans, X.-C. Zhang, *Detection and identification of explosive RDX by THz diffuse reflection spectroscopy.* Optics Express, 2006. **14**(1): p. 415–423
9. Zhong, H., A. Redo-Sanchez., X.-C. Zhang, *Identification and classification of chemicals using terahertz reflective spectroscopic focal-plane imaging system.* Optics Express, 2006. **14**(20): p. 9130–9141.
10. Wang, Y., Z. Zhao, Z. Chen, K. Kang, B. Feng, Y. Zhang, *Terahertz absorbance spectrum fitting method for quantitative detection of concealed contraband.* Journal of Applied Physics, 2007. **102**(11): p. 1131081–1131086.
11. Lippmann, R.P., *An introduction to computing with neural nets.* IEEE ASSP, 1987: p. 4–22.
12. Zorych, I., Yew Li Hor, Alexander M. Sinyukov, Zoi-Heleni Michalopoulou, Robert B. Barat, Dale E. Gary, and John F. Federici *A Statistical Approach to RDX Detection with THz Reflection Spectra*, in *CAMS Techical Report Series 2008–2009*. 2008, New Jersey Institute of Technology.
13. Mittleman, D.M., *Terahertz Imaging*, in *Sensing with Terahertz Radiation*, D.M. Mittleman, Editor. 2003, Springer. p. 117–153.
14. Liu, Z., Ke Su, Dale E. Gary. John F. Federici, Robert B. Barat, Zoi-Heleni Michalopoulou, *Video-rate terahertz interferometric and synthetic aperture imaging.* Applied Optics, 2008: p. 3788–3795.
15. Hastie, T., R. Tibshirani, J. Friedman, *The Elements of Statistical Learning*. 2001: Springer.
16. Huang, Y.S., C. Y. Chen, *A Method of Combining Multiple Experts for the Recognition of Unconstrained Handwritten Numerals.* IEEE Transactions on Pattern Analysis and Machine Intelligence. **17**: p. 90–94.